Inner-shell photoionization of excited lithium

H. L. Zhou,[1] S. T. Manson,[1] L. Vo Ky,[2] P. Faucher,[2] F. Bely-Dubau,[2] A. Hibbert,[3] S. Diehl,[4] D. Cubaynes,[4] J.-M. Bizau,[4] L. Journel,[4] and F. J. Wuilleumier[4]

[1]*Department of Physics and Astronomy, Georgia State University, Atlanta, Georgia 30303-3083*

[2]*UMR du CNRS 6529, Observatoire de la Côte d'Azur, Boîte Postale 4229, 06304 Nice Cedex, France*

[3]*Queen's University of Belfast, Belfast BT7 1NN, United Kingdom*

[4]*Laboratoire de Spectroscopie Atomique et Ionique, URA 775 du CNRS, Université Paris–Sud, Bâtiment 350, 91405 Orsay Cedex, France*

(Received 22 July 1998)

Calculations of inner-shell photoionization of $1s^2 2p\ ^2P^o$ and $1s^2 3p\ ^2P^o$ Li excited states have been performed using recent developments of the *R*-matrix code with a 29-term target representation for incident photon energies up to 165 eV, with particular emphasis on multiple electron processes. Partial and total cross sections are given for a number of excitation processes including the lower members of 19 hollow atom resonance series. The results are compared with recent experimental measurements of the lowest $2s2p^2\ ^2L^e$ resonance of even-parity hollow lithium states produced by photoexcitation of laser-excited lithium atoms. Experiment and theory are in excellent agreement on a relative scale. The enhancement of the shake-up process increases with initial state excitation, up to 500% over that of the ground state for $1s^2 3p\ ^2P^o$. Good agreement is also obtained for *K*-shell photoionization when comparing branching ratios with available experimental results. [S1050-2947(99)08801-0]

PACS number(s): 32.80.Fb, 32.80.Hd

I. INTRODUCTION

The photoionization of Li is of great interest because it is the simplest system that contains both an inner and outer shell in the ground state. In addition, since the Li atom consists of only three electrons, one has the possibility of treating it with substantial accuracy, from a theoretical point of view, thereby attaining a detailed understanding of the photoabsorption process in this three-electron system. Of particular interest is inner-shell photoionization and the resulting atomic dynamics, particularly with regard to the ''response'' of the outer-shell electron on inner-shell photoabsorption. Theoretical calculations for the process of inner-shell photoionization of atomic lithium in its ground state were the subject of two previous papers [1,2], hereafter denoted paper I and paper II, respectively. These calculations were performed using recent developments of the *R*-matrix code with a target representation including up to 29 states. Paper I was restricted to the photon energy region up to 140 eV, including the analysis of the resonances in the partial cross sections due to the $1snln'l'$ autoionizing states, whereas paper II was extended to the photon energy region of hollow atomic states. For this latter case, to our knowledge the calculations were the first computations of inner-shell photoionization cross sections including such resonances. The excellent agreement between theoretical and measured results [3–7] for both partial and total photoionization cross sections emphasizes the quality of the theoretical model. Another recent calculation of the photoionization cross section from the ground state of lithium, including the analysis of resonances between $1s2s\ ^3S$ and $1s2p\ ^3P$ ionization thresholds, was recently performed [8] using the saddle-point method, giving good agreement with our results [1] and experiment.

In recent work, new phenomenology has been predicted in the $1s$ photoionization of excited Li [9]; calculations of photoionization from the $1s^2 3p\ ^2P$ excited state show a dominant cross section to the $1s4p\ ^3P$ channel, revealing that the two-electron process of ionization plus excitation (so-called shake-up) dominates the single-electron direct photoionization. Although these multiconfiguration Hartree-Fock (MCHF) calculations omitted coupling among channels, it was noted that the results were due primarily to relaxation of the final-state orbitals, thereby significantly enhancing the overlap of the initial state $3p$ with the final state $4p$; thus, away from threshold, the omission of interchannel coupling should not be a major factor. Similar calculations on the $1s^2 2p\ ^2P$ excited state do not result in so large a contribution for the shake-up process. Experimental results were obtained for inner-shell photoionization of $2p$-excited Li atoms [10] over the photon energy extending from 83 to 112 eV. The experimental photoelectron spectra show two groups of lines clearly, a first group which correspond to direct photoionization of a $1s$ electron ($1s2p\ ^{1,3}P$ final states) and a second one which corresponds to the excitation of the $2p$ valence electron to the $n=3$ shell accompanying photoionization of the $1s$ electron. The important experimental result deduced from this spectrum was the very strong enhancement of the satellite processes of the excited Li atom, the strongest then obtained, when comparing to the ground state. For example, a ratio of 0.76 ± 0.10 (against a value of 0.25 ± 0.05 in the ground state) was measured between the intensity of the sum of all ($n=3$) satellite lines and the intensity of the main line for excited Li. This result followed the trend previously obtained for sodium and potassium atoms [11–13]. These theoretical and experimental results provide significant motivation to extend our calculations to the $1s^2 2p$ and $1s^2 3p$ excited states of Li.

In addition, very recently, the first experimental results (to our knowledge) of even-parity hollow lithium states produced by photoexcitation of laser-excited lithium atoms were measured using photoelectron spectroscopy [14]. The experi-

mental measurements were performed at the Advanced Light Source (ALS) in two energy ranges covering the $2s2p^2\,^2L^e$ and $2p^23d\,^2L^e$ resonances. Preliminary results of some partial cross sections obtained with the present mathematical model [14] showed that experimental and theoretical results are in very good agreement. This gives further motivation to perform a more detailed calculation for the odd-parity excited initial states.

The purpose of the present paper is to calculate the various atomic parameters which characterize the process of photoionization (partial and total cross section, branching ratio, asymmetry parameter, β) for the $1s^22p$ and $1s^23p$ excited states of the Li atom and for incident photon energies up to 165 eV. This energy range includes the $1snln'l'$ resonances for $n\leqslant 4$ at low energies and the $2l2l'n''l''$ resonances at high energies. The mathematical model chosen to represent the target is the same as used in paper II. We have to note, however, that the 19-term target used in paper I also gives quite good results for incident photon energies below 140 eV. The present calculations are compared with the previous MCHF theoretical results [9] outside the resonance regions for photon energies below 120 eV. For higher energies corresponding to hollow atomic states, comparisons are also made with experimental measurements obtained at the ALS [14].

II. PHOTOIONIZATION CROSS SECTIONS

As discussed in paper II, in order to obtain a model which correctly represents the physical process over a large range of photon energies up to 165 eV, the close-coupling (CC) expansion of the Li^+ target is represented by 29 states obtained from the first ten configurations $1s^2$, $1snl$, $n=2,3,4$, and $l=s,p,d,f$, as well as $2s^2$, $2s2p$, $2p^2$, $2s3s$, $2s3p$, and $2p3s$. The CI expansion includes up to 151 basic configurations giving 369 configuration couplings to construct the 29 target states. The radial functions for the orbitals are evaluated using the code CIV3 [15] and are expressed in Slater-type analytic form. Such a representation allows us to obtain calculated target state energies which compare well with experiment (see Table III, paper II).

In this paper, partial photoionization cross sections are calculated for the following processes:

$$1s^22p\,^2P^o+h\nu\rightarrow[nln'l'+e(kl'')]^2S^e,^2P^e,^2D^e, \quad (1)$$

$$1s^23p\,^2P^o+h\nu\rightarrow[nln'l'+e(kl'')]^2S^e,^2P^e,^2D^e, \quad (2)$$

where the $nln'l'$ configurations are given above and correspond to the 29 Li^+ target states.

Initial bound states (symmetry $^2P^o$) and final continuum states (symmetries $^2S^e$, $^2P^e$, and $^2D^e$) of the $(N+1)$-electron system are calculated on the same footing using the R-matrix method with the following parameters: R-matrix radius $a=30.2a_0$, 38 continuum basis functions for each orbital angular momentum; l'' of 0, 1, 2, and 3 were included. The wave function for the $(N+1)$-electron system of total symmetry $SL\pi$ is written [see Equation (1) of paper II for definition of notation]

$$\Psi^{\mathrm{SL}\pi}=A\sum_{i=1}^{N^F} c_i\phi_i(S_iL_i;\mathbf{x}_1,\ldots,\mathbf{x}_N,\hat{\mathbf{x}}_{N+1})F(k_il_i;r_{N+1})r_{N+1}^{-1} + \sum_{j=1}^{N^B} d_j\Phi_j^{SL\pi}. \quad (3)$$

TABLE I. $Li^+ + e^-$: Number of channels and corresponding bound terms for each $LS\pi$ state.

State	N^{ch}	N^B
$^2P^o$	44	921
$^2S^e$	28	486
$^2P^e$	19	608
$^2D^e$	46	1004

Table I gives, for the four $SL\pi$ symmetries of the $(N+1)$-electron system, the number N^B of bound terms built from the 369 coupling configurations retained in the close-coupling (CC) expansion as well as the number N^{ch} of channels which give rise to these bound terms, where N^F in Eq. (3) is equal to $N^{\mathrm{ch}}\times 38$.

As discussed in papers I and II, a severe test for the mathematical model of the combined $Li^+ + e^-$ system is provided by the eigenenergies of the members of the three series $1s^2ns\,^2S^e$, $1s^2np\,^2P^o$, and $1s^2nd\,^2D^e$. Table II compares experimental and calculated effective quantum numbers for the third series $1s^2nd\,^2D^e$ (results for the two other series $1s^2ns\,^2S^e$ and $1s^2np\,^2P^o$ are given in Table VI, paper I). It is seen that our results are very close to experiment.

Another good test of the theory is a comparison with experimental oscillator strengths for the combined $Li^+ + e^-$ system where the results showed excellent agreement (see paper I). Finally, the mathematical model is checked by the agreement of the results in the length and velocity formulations.

The present calculations have been performed for photon energies up to 167 eV. In order to better compare the present results with previous calculations or experimental measurements, the photon energy range will be considered in two regions: (a) the region below 140 eV which includes the $1snln'l'$ Rydberg resonance series, and (b) the region of the first hollow atomic states between 140 and 167 eV corresponding to the $2ln'l'n''l''$ Rydberg resonance series.

TABLE II. $Li^+ + e^-$: Effective quantum numbers n^* of $1s^2nd\,^2D^e$ series and comparison with experimental values of Johansson [24].

n	3	4	5	6	7	8	9
n^* (calc.)	2.989 92	3.995 64	4.995 64	5.995 47	6.995 51	7.995 54	8.995 57
n^* (expt.)	2.998 53	3.998 33	4.998 23	5.998 18	6.998 13	7.998 02	8.998 06

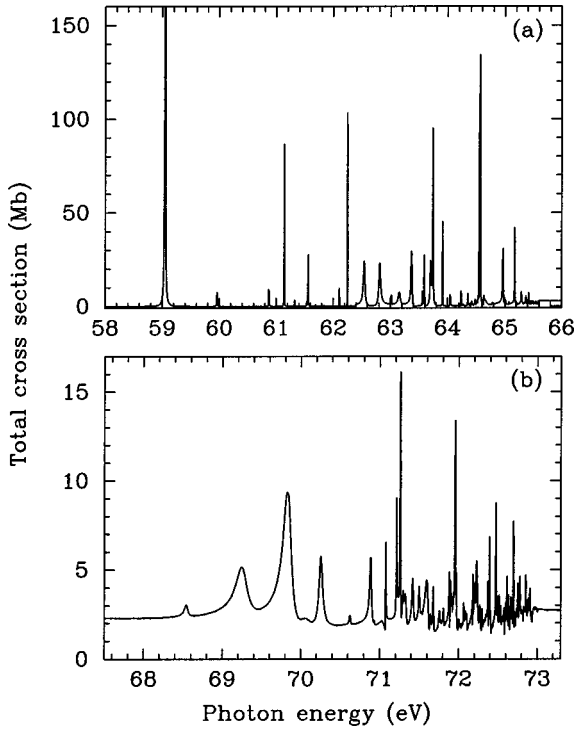

FIG. 1. Theoretical total cross section (Mb) for photoionization of the $1s^2 2p\ ^2P$ lithium excited state in two photon energy ranges: (a) region of the $1s2ln'l'$ Rydberg series, (b) region of the $1s3ln'l'$ Rydberg series. Results in length form and in velocity form are superimposed.

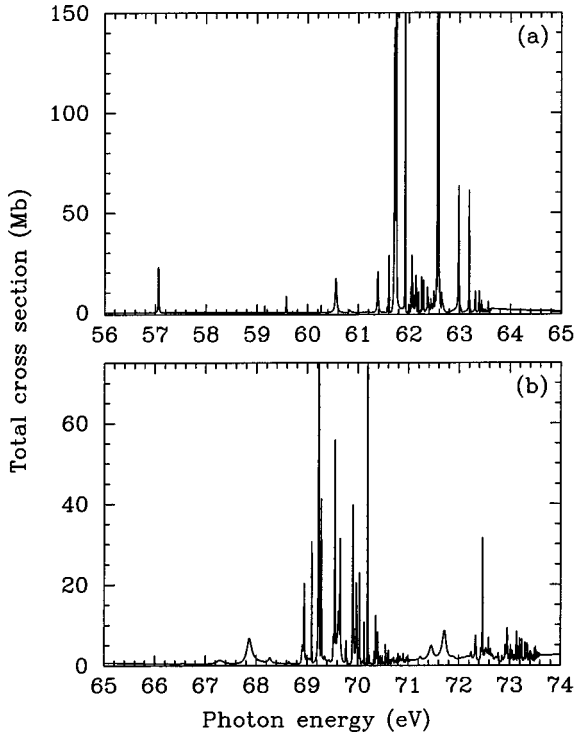

FIG. 2. Theoretical total cross section (Mb) for photoionization of the $1s^2 3p\ ^2P$ lithium excited state in two photon energy ranges: (a) region of the $1s2ln'l'$ Rydberg series, (b) region of the $1s3ln'l'$ Rydberg series. Results in length form and in velocity form are superimposed.

A. Cross sections for incident photon energies below 140 eV

Our calculated results for the total photoionization cross sections for $1s^2 2p$ and $1s^2 3p$ in the $1snln'l'$ resonance region below the $1s$ ionization threshold are given in Figs. 1 and 2, respectively. Figures 1(a) and 2(a) show the $1s2ln'l'$ resonances while Figs. 1(b) and 2(b) present the $1s3ln'l'$ series. Unfortunately, there are no experimental investigations of those resonances. The results for length and velocity formulations are essentially exactly the same, indicating the quality of the calculation. Note that exactly the same resonances are seen in both sets of curves, shifted by the 1.980 eV difference in binding energy. However, although the final-state resonance positions and widths do not depend upon the initial state, the oscillator strengths and shapes do. The calculations are done on a 5×10^{-4} Ry (0.0068 eV) energy mesh to insure the characterization of each resonance. The detailed assignments of these resonances, along with the parameters of each, will be given in a subsequent publication.

Above this resonance region, the present R-matrix cross sections are presented in the 70–140 eV photon energy range for photoionization of the excited $1s^2 2p$ and $1s^2 3p$ states in Figs. 3 and 4, respectively, with the cross sections leaving the Li^+ ion in any of the $1snp\ ^{1,3}P$ $(n=2,3,4)$ states given individually. The thresholds are given in Table III. Looking first at the $1s^2 2p$ cross sections in Fig. 3, the dominant channel is seen to be the $1s2p\ ^3P$ state Li^+ over the entire energy range. The $1s2p\ ^1P$ state cross section is less important just due to statistical weight; in the absence of any dynamical effects, the ^1P cross section is just $\frac{1}{3}$ of the ^3P. Further, Fig. 3 reveals that the ionization plus excitation cross sections to the $1s3p\ ^{1,3}P$ states of Li^+ are smaller than their $1s2p$ counterparts. Thus the single-particle ionization process dominates over ionization plus excitation, which is generally the case.

Also shown in Fig. 3 are the earlier MCHF results [9] which show excellent agreement for all four cross sections at the highest energies presented, indicating that coupling between the various channels is not terribly important at the higher energies. But near the thresholds, the MCHF results are seen to be rather unreliable, even as to their shapes,

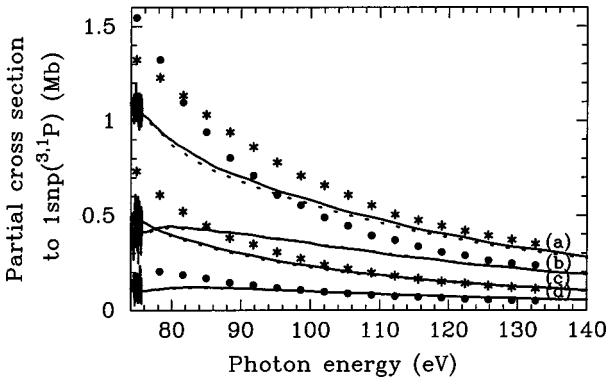

FIG. 3. Partial cross sections for photoionization of the $1s^2 2p\ ^2P$ lithium excited state leaving the Li^+ ion in an excited state of configuration $1snl$ at photon incident energies outside the resonance regions. (a) $1s2p\ ^3P$, (b) $1s3p\ ^3P$, (c) $1s2p\ ^1P$, (d) $1s3p\ ^1P$. Present results: full line, length form; dotted line, velocity form. (∗) Corresponding theoretical calculations from Felfli and Manson [9]: (∗) for (a) and (c), (●) for (b) and (d).

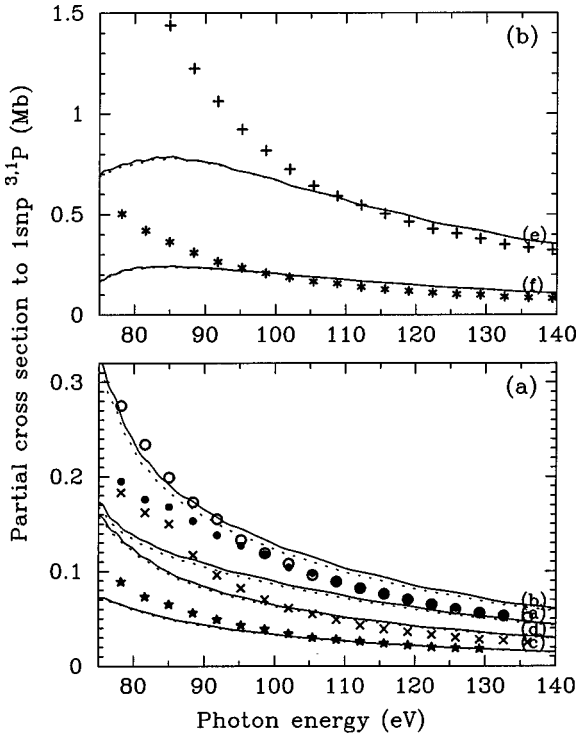

FIG. 4. Partial cross sections for photoionization of the $1s^2 3p\ ^2P$ lithium excited state leaving the Li^+ ion in an excited state of configuration $1snl$ at photon incident energies outside the resonance regions. (a) $1s2p\ ^3P$, (b) $1s3p\ ^3P$, (c) $1s2p\ ^1P$, (d) $1s3p\ ^1P$, (e) $1s4p\ ^3P$, (f) $1s4p\ ^1P$. Present results: full line, length form; dotted line, velocity form. The corresponding theoretical calculations from Felfli and Manson [9] are given, respectively, by (●) for curve (a), (○) for curve (b), (⋆) for curve (c), (×) for curve (d), (+) for curve (e), and (∗) for curve (f).

showing the crucial importance of interchannel coupling in the energy region of the thresholds.

The situation is dramatically different for the cross sections for photoionization of the $1s^2 3p$ excited state, shown in Fig. 4, where the dominant cross section over the entire region is the $1s4p\ ^3P$ channel; ionization plus excitation. At the higher energies, the next largest cross section is the $1s4p\ ^1P$, indicating just how dominant this configuration really is. Again, as in the $1s^2 2p$ case, the MCHF results are in fairly good agreement at the highest energies, but are unreliable close to the thresholds. In any case, at the highest energies, the MCHF results are a reasonably good approximation to the present *R*-matrix cross sections for both $1s^2 2p$ and $1s^2 3p$ photoionization. Therefore, the explanation of the higher energy results based upon the simpler MCHF calculation is justified [9].

Briefly, the principal term in the dipole matrix element at the higher energies for each of the $1s^2 np \rightarrow 1sn'pkp$ $^{1,3}S,P,D$ allowed transitions is, apart from angular factors, given by

$$\langle 1s_i|1s_f\rangle\langle np_i|n'p_f\rangle\langle 1s_i|r|kp_f\rangle,$$

where the subscripts refer to initial- and final-state wave functions, respectively. For each of the initial states, the only significant change in the dominant term of the matrix element comes from the middle factor, $\langle np_i|n'p_f\rangle$. For the $1s^2 2p$ case, the $\langle 2p_i|2p_f\rangle$ factor is much larger than $\langle 2p_i|3p_f\rangle$ so that the cross section, which is proportional to the square of the matrix element, is larger for the $1s2p$ final state as seen in Fig. 3. But for the $1s^2 3p$ case, the $\langle 3p_i|4p_f\rangle$ gives the largest overlap. This is because the $3p_i$ electron ''sees'' a charge of unity, the Li nucleus screened by the two $1s$ electrons, but the final $n'p_f$ states ''see'' a charge of 2, a factor of 2 increase, with one of the $1s$ electrons removed; this causes the $n'p_f$ orbitals to be significantly more compact than their initial-state counterparts. In this case, the $4p_f$ function occupies the same region of space as $3p_i$, so the overlap is maximized for $\langle 3p_i|4p_f\rangle$. For the $1s^2 2p$ excited initial state, the removal of the $1s$ electron still changes the asymptotic effective charge 1, but owing to the penetration of the $2p$ into the core region, the change is nowhere near a factor of 2 as it is for the $3p$. This is why $1s^2 2p$ photoionization does not exhibit dominance of ionization plus excitation.

At the lower energies, these cross sections are significantly more complicated; owing to the coupling of channels, simple overlap arguments are quite insufficient to explain the details of the cross section. But the general idea, that the single electron process dominates the $1s^2 2p$ photoionization cross section despite interchannel coupling and autoionizing resonances, remains true, as seen in Fig. 3. And the two-electron process dominates the $1s^2 3p$ photoionization cross section down to threshold, as seen in Fig. 4.

To explicitly investigate the importance of satellite, two-electron processes, the branching ratio of partial cross sections between satellite and main lines, summed over multiplets, for Li $1s^2 2p\ ^2P$ excited-state photoionization is shown in Fig. 5. The ratios $[\sigma(1snl^3L)+\sigma(1snl^1L)]/[\sigma(1s2p(^3P)+\sigma(1s2p\ ^1P)]$ are shown for $nl=3s,3p,3d$, along with their sum which represents the branching ratio to all $n=3$ final states. These results show that the ''shake-up'' process, where the $2p$ in the initial state is excited to a $3p$ in the final state, dominates the two-electron processes at higher energies. At the lower energies, while the ''shake-up'' cross section is still the largest, by no means does it dominate, as seen in Fig. 5. This further confirms that the two-electron processes are extremely complicated in the threshold region.

In addition, it is clearly seen that, in Fig. 5, although the $n=3$ satellites do not dominate the cross section, they are

TABLE III. Binding energies (in eV) of the first ionization thresholds relative to the first excited state $1s^2 2p$ in atomic lithium.

State	$1s^2\ ^1S$	$1s2s\ ^3S$	$1s2s\ ^1S$	$1s2p\ ^3P$	$1s2p\ ^1P$	
E (eV)	3.546	62.386	64.314	64.649	65.604	
State	$1s3s\ ^3S$	$1s3s\ ^1S$	$1s3p\ ^3P$	$1s3d\ ^3D$	$1s3d\ ^1D$	$1s3p\ ^1P$
E (eV)	72.142	72.646	72.729	72.942	72.946	73.014

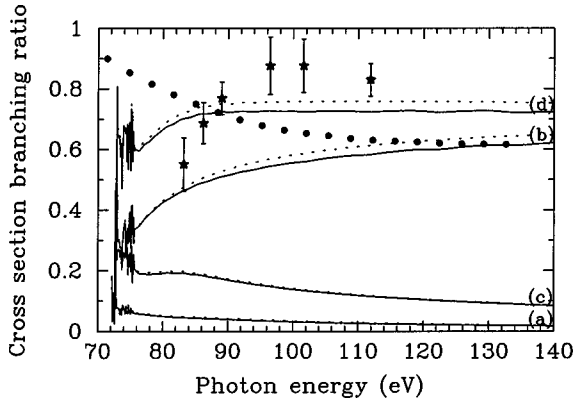

FIG. 5. Partial cross-section branching ratio for photoionization of the $1s^2 2p\ ^2P$ lithium excited state at energies outside the resonance regions. (a) $\sigma(1s3s(^{3,1}S))/\sigma(1s2p(^{3,1}P))$, (b) $\sigma(1s3p(^{3,1}P))/\sigma(1s2p(^{3,1}P))$, (c) $\sigma(1s3d(^{3,1}D))/\sigma(1s2p(^{3,1}P))$, and (d) total $\sigma(n=3)/\sigma(1s2p(^{3,1}P))$ branching ratio. Present results: full line, length form; dotted line, velocity form. (●) Theoretical calculations from Felfli and Manson [9] corresponding to the ratio (b). (⋆) Experimental results from Journel [10] corresponding to the sum (d).

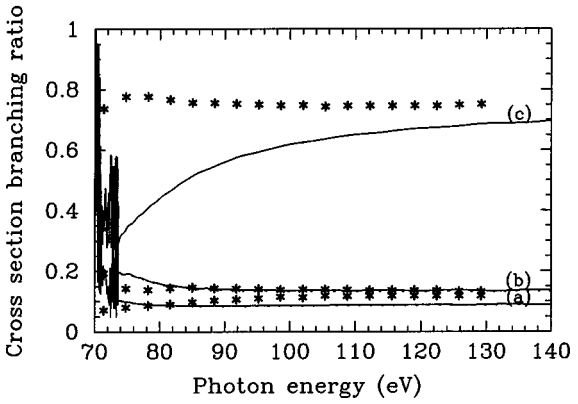

FIG. 6. Partial cross-section branching ratio for photoionization of the $1s^2 3p\ ^2P$ lithium excited state at energies out of the resonance regions. (a) $\sigma(1s2p(^{3,1}P))/\sigma$ (total), (b) $\sigma(1s3p(^{3,1}P))/\sigma$ (total), and (c) $\sigma(1s4p(^{3,1}P))/\sigma$ (total), with σ (total) $=\sum_{n=2}^{n=4}\sigma(1snp(^{3,1}P))$. Present results: full line, length form; dotted line, velocity form. (∗) Corresponding theoretical calculations from Felfli and Manson [9].

more than 70% of the main line at the higher energies, and only slightly less in the $1s$ threshold region. Thus, the notion of them being small satellites is hardly appropriate.

The experimental results [10] for the total $(3s+3p+3d)$ $n=3$ branching ratio for $1s^2 2p$ photoionization are also shown in Fig. 5, where good agreement with the calculation is seen. They reproduce well the calculated energy dependence of the branching ratio, although there are some differences in the quantitative values at low- and high-photon energies. Further measurements with higher spectral resolution are needed to resolve the individual $(1s3l)$ components of the $n=3$ photoelectron line. The results of the MCHF calculation for the $1s3p$ final state are also shown in Fig. 5. Excellent agreement with *R*-matrix results is seen at the higher energies. However, in the threshold region the MCHF result predict a completely wrong behavior in comparison with the *R*-matrix and experimental results, owing to the omission of interchannel coupling.

Similar branching ratios are presented for $1s^2 3p$ photoionization for $1s2p$, $1s3p$, and $1s4p$ final configurations of Li^+ as a fraction of the total cross section in Fig. 6. At the higher energies it is seen that the $1s4p$ final states are about 70% of the total and vastly overshadow the $1s3p$ final states. The $1s4p$ cross sections are still the largest near threshold but not nearly as dominant as they are at high energy. Further, the MCHF results are quite reasonable at high energy, but not really adequate near threshold, as in the previous case, as interchannel coupling is omitted in the MCHF calculation.

For the reasons discussed above in connection with Fig. 4, it is clear that as the initial state becomes more and more excited, so that the outer electron penetrates the core less deeply, the two-electron ionization plus excitation process should become increasingly important relative to ionization alone. For instance, the ratio, summed over multiplets, $\sigma(1s(n+1)l)/\sigma(1snl)$ for $nl=2s$, $2p$, and $3p$, is found to be 0.25, 0.60, and 5.0 in the high-energy region. This confirms the previous discussion, as well as the prediction based upon MCHF calculations [9]. It is clear that this trend will continue with still more highly excited initial states.

The expression for the asymmetry parameter β which relates the differential cross section $d\sigma(L_i S_i \rightarrow L_f S_f)/d\hat{k}_f$ to the integrated cross section σ is given in paper I. The asymmetry parameter can be obtained from our theoretical results for any transition leaving the ion in any state given in Table III of paper II and these will be discussed in detail in a future publication. To give a flavor of the results obtained from our β calculations, the situation for the photoionization of the excited $1s^2 2p\ ^2P^o$ initial state of Li leading to excited states (a) $1s2p\ ^{1,3}P$, (b) $1s3s\ ^{1,3}S$, (c) $1s3p\ ^{1,3}P$, and (d) $1s3d\ ^{1,3}D$ are shown in Fig. 7 for the singlet and triplet ionic states. The β for the singlet ionic states are qualitatively similar to those for the triplets, but a close inspection reveals significant quantitative differences, particularly in the resonance and threshold regions. This indicates dynamical differences between the singlet and triplet channels in these regions.

For transitions to the $1snp\ ^{1,3}P$ final states, the predominant transition is $1s \rightarrow kp$ which can couple to the core in three ways giving $1snpkp$ $(^2S^e, ^2P^e, ^2D^e)$ final states of the Li^+ plus photoelectron system (with the introduction of correlation, $1snpkf\ ^2D^e$ final states are also possible, but are quite small). In the threshold region, above the resonances where dynamical effects in the three channels differ, predominantly due to exchange, the interference among the channels results in a β which is slightly less than 2. Away from threshold, where the effects of exchange fall off rapidly with energy, the dynamics of each of these channels is the same so that no interference can occur. Then, from general considerations [16], β tends rapidly towards 2, which is also the result of the simple Cooper-Zare form [17]. This rapid approach to $\beta=2$ is seen clearly for both ^1P and ^3P cores in Fig. 7.

In the resonance region near the thresholds we find both large excursions of β from 2 as well as very significant differences between ^1P and ^3P channels, as seen clearly in Fig. 7. This behavior results because, although there are reso-

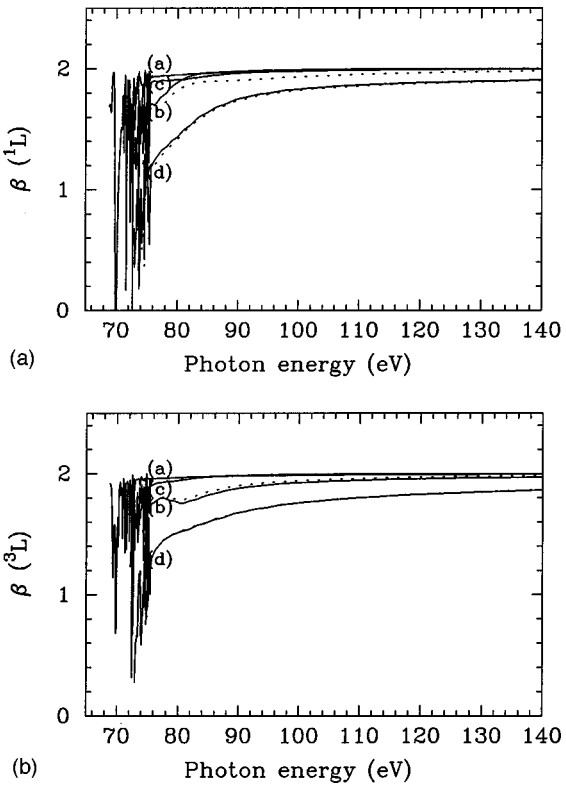

FIG. 7. Asymmetry parameter β for photoionization of the $1s^2 2p\ ^2P$ lithium excited state leaving the Li^+ ion: (a) (^1L) states, (b) (^3L) states. (a) $1s2p$, (b) $1s3s$, (c) $1s3p$, (d) $1s3d$. Results in length form and velocity form are superimposed.

nances in each of the $^2S^e$, $^2P^e$, and $^2D^e$ channels, they occur at slightly different energies; thus, at any given energy, there can be dramatic differences in the amplitudes (and phases) among the three $^2L^e$ channels so that dramatic interferences can occur, resulting in large swings in β. Further, since the details of the resonances differ between the ^1P and ^3P manifolds, the details of β will differ as well, just as seen in Fig. 7.

In the case of the $1s3s\ ^{1,3}S$ channels, detailed analysis [16] shows that only $1s3sks\ ^2S^e$ and $1s3skd\ ^2D^e$ states are possible for the Li^+ plus photoelectron system; the Cooper-Zare form [17] is exact here, i.e.,

$$\beta = \frac{2R_d^2 - 4R_d R_s \cos(\sigma_d + \delta_d - \sigma_s - \delta_s)}{R_s^2 + 2R_d^2}, \qquad (4)$$

where R_d and R_s are the absolute values of the effective radial dipole matrix elements, and σ_l and δ_l are the Coulomb and non-Coulomb phases of these matrix elements. In the resonance region, the resonances in the $^2S^e$ and $^2D^e$ channels, occurring at different energies, cause the rapid large-amplitude variations of β. Just above the resonance region, the rapid change in the Coulomb phase shift difference, a general consequence of interference between continuum waves of different angular momentum in the near-threshold region [18], causes the relatively rapid variation of β with energy; the differences between the ^1S and ^3S channels seen in Fig. 7 indicate just how different the photoionization dynamics are in this energy region. At the higher energies, the calculation finds that $R_d \approx R_s$ over a fairly broad range. In addition, at the higher energies, the Coulomb phase shifts (and, thus, their differences) get very small. For the non-Coulomb phase shifts, in the photon energy region 90–140 eV, $\delta_d \approx 0$ and $\delta_s \approx \pi$ so that the total phase difference is about π and the cosine in Eq. (4) is -1; putting these together yields $\beta \approx 1.97$ from Eq. (4), the value that is seen for the higher energies in Fig. 7. Note that the approach to roughly $\beta = 2$ in these channels is only accidental, and not the consequence of any general principles. In fact, at still higher energies, as δ's decrease (all $\delta_l \to 0$ as $h\nu \to \infty$), β for the $^{1,3}S$ channels will deviate significantly from $\beta = 2$; the $^{1,3}P$ channels will continue to exhibit $\beta = 2$, however.

For the $1s3d\ ^{1,3}D$ final states, the situation is the most complicated of the cases discussed since there are five possible final Li^+ plus photoelectron states: $1s3dks\ ^2D^e$, $1s3dkd\ ^2S^e$, $^2P^e$, $^2D^e$, and $1s3dkg\ ^2D^e$. Transition amplitudes to the last are quite small and have not been included in our calculation. At the lower energies there is interference among the three *kd* partial waves, similar to the cases of $1snp\ ^{1,3}P$ discussed above. There is also interference between the *kd* channels and *ks* channel. This leads to complex resonance behavior and, above the resonance region, rapid variation owing to the rapid change in the Coulomb phase-shift difference. In addition, β is not close to 2 and is rather different for ^1D and ^3D, as seen in Fig. 7. At the higher energies, the situation becomes simpler, but still more complicated than any of the other cases discussed. The main contribution to β comes from the interaction of the *ks* with the *kd* channels, and, for exactly the same reasons as in the $1s3s$ case, this term is roughly 2 at the higher energies. Another contribution, whose weight is only 14% of the above term, arises from the interferences among the *kd* channels and gives a constant value of 2/7. Putting these contributions together yields a β at the higher energies of slightly greater than 1.8, just as seen in Fig. 7. The fact that the interferences among the *kd* channels is still important at these energies indicates that the exchange interactions in these channels remain important to much higher energies than was the case in the $1s2pkp$ channels discussed above. A more detailed discussion of β for these and other channels will be presented in a future publication.

B. Cross sections for photon incident energies between 140 and 165 eV

Photoexcitation yielding hollow lithium atoms has been the subject of intense experimental and theoretical interest in recent years. However, investigation of hollow lithium states has chiefly been restricted to excitation from the ground state ($^2S^e$). Because of the dipole selection rules, only the formation of odd-parity hollow states ($^2P^o$) was allowed. The first measurements of even-parity hollow lithium states produced by photoexcitation of laser-excited lithium atoms and using photoelectron spectroscopy was recently reported [14]. Partial cross sections were measured for photoionization of the $1s^2 2p$ excited lithium atom into the $1s2p\ ^3P^o$ and $^1P^o$ final ionic states over the energy ranges covering the $2s2p^2\ ^2D^e$ and $^2P^e$ resonances as well as into the $1s3l\ ^{3,1}L$ around the $2p^2 3d\ ^2D^e$ and $^2P^e$ resonances. These experimental measurements were compared with corresponding preliminary theoretical *R*-matrix calculations obtained from the present

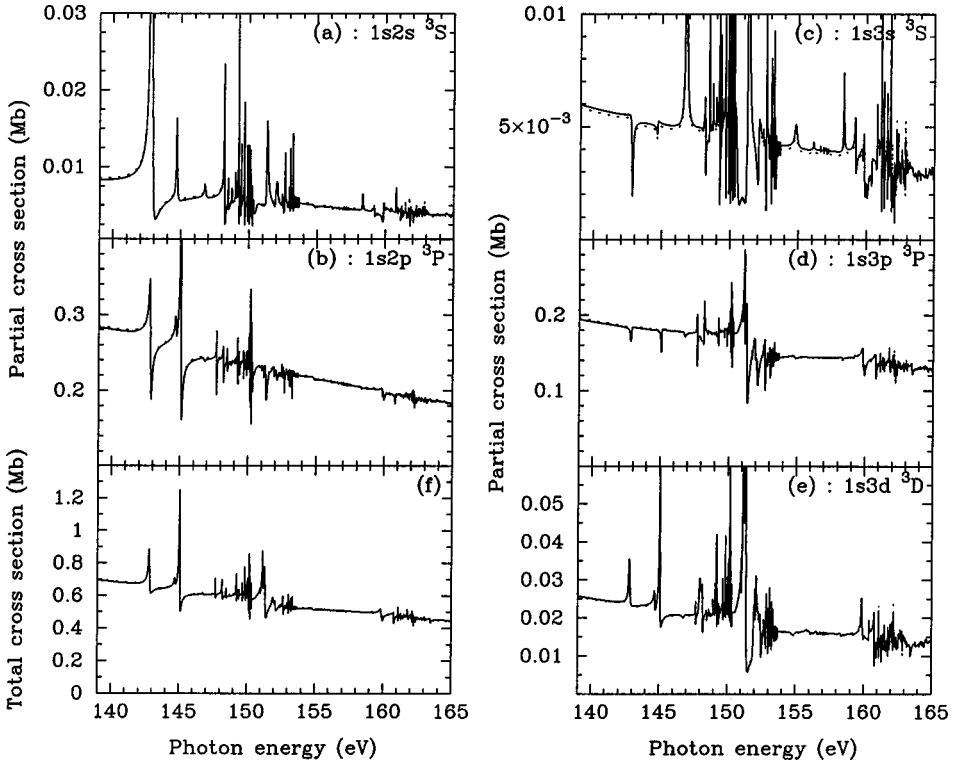

FIG. 8. Partial cross sections for photoionization of the $1s^2 2p\ ^2P$ lithium excited state leaving the Li^+ ion in a ^3L excited state for the following configurations: (a) $1s2s$, (b) $1s2p$, (c) $1s3s$, (d) $1s3p$, and (e) $1s3d$. The curve (f) represents the total photoionization cross section. Results in length and velocity forms are superimposed.

model. Agreement of partial cross sections is quite good on a relative scale, the *R*-matrix energy values being slightly lower than the experimental ones. For each partial cross section to a given ionic state, the *R*-matrix calculation of the contribution to each final state $^2D^e$, $^2P^e$, or $^2S^e$ allows us to assign clearly the resonances corresponding to each $SL\pi$ final state.

The results of the *R*-matrix calculation are given in Figs. 8 and 9 for the photoionization of $1s^2 2p$ and $1s^2 3p$ initial excited states of Li, respectively, in the 140–165 eV energy region, the region of $2l2l'n''l''$ ''hollow'' atom resonances. Each figure presents the total cross section along with the partial cross sections for five of the largest channels, i.e., cross sections for leaving the Li^+ ion in various final states. The cross sections for the smaller channels which were calculated are, of course, included in the total but are not shown individually, nor is the cross section to the ''subchannels'' corresponding to each $SL\pi$ designated final state.

The results shown in Figs. 8 and 9 demonstrate the importance of the ionization plus excitation process in this energy range as well, particularly for the $1s^2 3p$ initial state. For the $1s^2 2p$ initial state, it is seen from Fig. 8 over the entire energy region that although the single electron process leading to the $1s2p\ ^3P$ final state has the largest cross section, it is only 50% larger than the $1s3p\ ^3P$ cross section and certainly less than half of the total. For the $1s^2 3p$ initial state, it is striking how dominant is the two-electron transition to the $1s4p\ ^3P$ state, as was the case in the lower energy range; the $1s4p\ ^3P$ partial cross section is seen in Fig. 9 to be a factor of 6 larger than the $1s3p\ ^3P$ single-particle cross section. Note that both length and velocity cross sections are shown in Figs. 8 and 9 and they virtually overlap, thereby giving confidence in the accuracy of the calculation, even in the energy range of the ''hollow'' atom resonances.

The importance of the ionization plus excitation (''shake-up'') process is summarized in Fig. 10, where the branching ratios, summed over final-state spin and orbital angular momentum, $\sigma(n=3)/\sigma(n=2)$ for the $1s^2 2p$ initial state and $\sigma(n=4)/\sigma(n=3)$ for the $1s^2 3p$ initial state, are shown. This ratio away from the resonances increases from about 0.7 for $1s^2 2p$ photoionization to roughly 6.0 for $1s^2 3p$, thus further supporting the contention that the two-electron process becomes more important when the initial state is more excited.

Note that the ratios vary considerably through the various resonances, even though exactly the same resonances must be excited in both the single-electron and the two-electron channels, owing to the fact that they both have precisely the same angular momentum geometry. As mentioned above, however, although the position and width of a resonance are invariant, the shape and strength are very much functions of the particular initial and final states. Thus, owing to the variations in resonance shape among the various channels, the ratio can exhibit substantial oscillations across a resonance; this explains the general behavior seen in the ratios in Fig. 10.

As mentioned previously, experimental measurements of even-parity hollow lithium states have been performed using photoelectron spectroscopy [14], and other experiments using photoion spectroscopy on excited lithium atoms are also in progress (see Ref. [14]). Since these experimental investigations are of the $1s^2 2p$ excited state of lithium, we present our theoretical results in greater detail for photoionization from this first excited lithium state in the photon energy

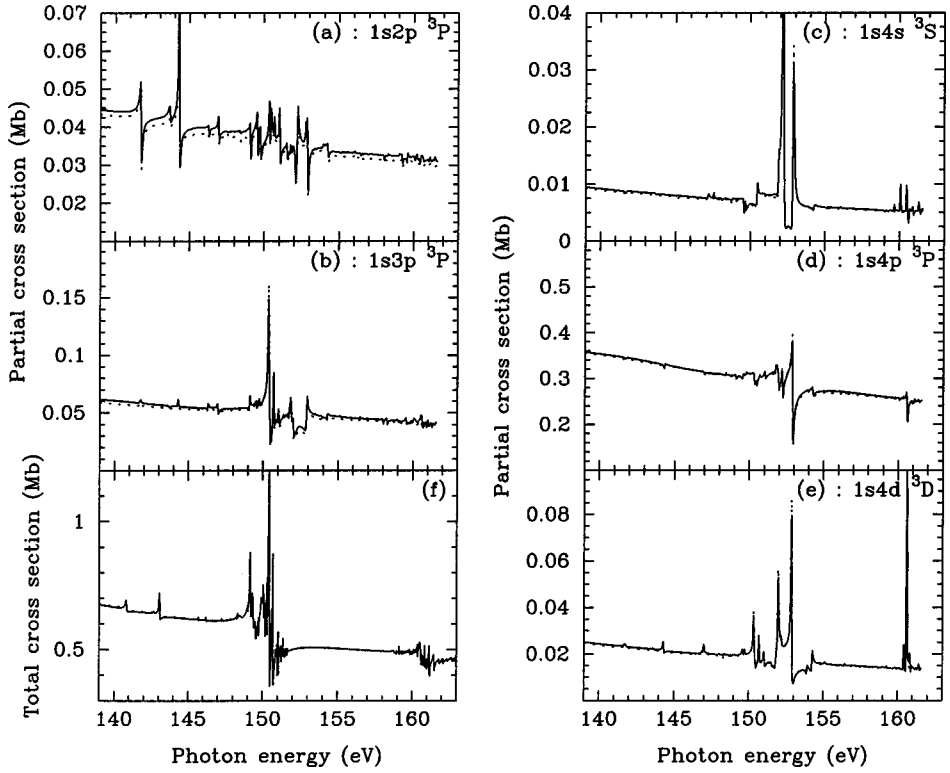

FIG. 9. Most intense partial cross sections for photoionization of the $1s^2 3p\ ^2P$ lithium excited state leaving the Li^+ ion in a ^3L excited state for the following configurations: (a) $1s2p$, (b) $1s3p$, (c) $1s4s$, (d) $1s4p$, and (e) $1s4d$. The curve (f) represents the total photoionization cross section. Results in length and velocity forms are superimposed.

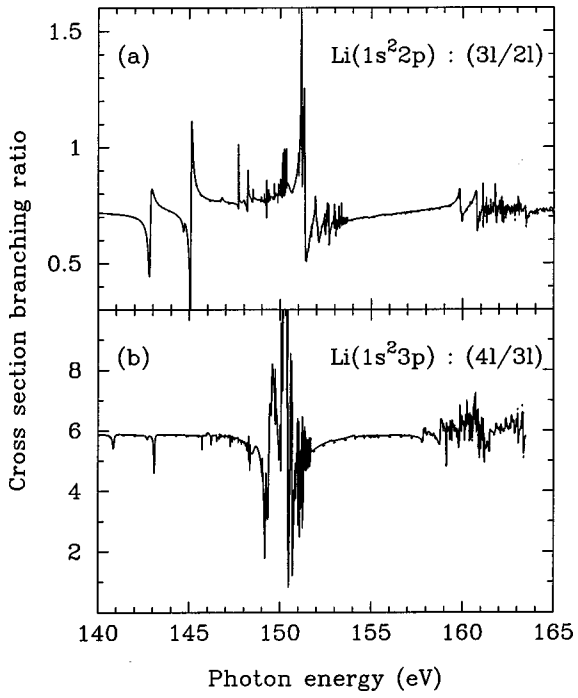

FIG. 10. Branching ratio between the sum of partial cross sections to a $1s3l$ final ionic state and the corresponding sum to a $1s2l$ final ionic state for photoionization from the $1s^2 2p$ Li initial state (a) and equivalent branching ratio between cross sections to a $1s4l$ final state compared to a $1s3l$ final state for photoionization from the $1s^2 3p$ excited initial Li state (b).

range which corresponds to the $2l2l'n''l''$ resonances between 140 and 160 eV. Table IV gives the R-matrix calculated energy positions of the $2l2l'$ ionization thresholds relative to this $1s^2 2p$ excited lithium state.

The calculated R-matrix cross sections for $1s^2 2p$ photoionization are shown, broken down by the final $SL\pi$ state, in Fig. 11 for transitions to each of the $^2D^e$, $^2P^e$, and $^2S^e$ of the total Li^+ ion plus photoelectron system, along with the total cross section, the sum over the three $SL\pi$ final states. This is a useful manner of scrutinizing the cross sections because each $LS\pi$ state includes a different set of resonances. Note that the background (continuum) cross sections for each of the $LS\pi$ channels are almost exactly in the statistical (or geometrical) $2L+1$ weighted ratio, 5:3:1. This implies that the nonresonant cross sections for the three $SL\pi$ channels have the same dynamics, i.e., radial wave functions, and only differ in (angular momentum) geometry.

The calculated cross-section results are compared in detail with a measured [19] ''hollow'' resonance in the $1s2p\ ^3P^o$ final channel in Fig. 12. The energy predicted is within 0.1 eV of the measured position, which tests further the accuracy of the wave functions employed in the calculation. Furthermore, the predicted resonance shape and strength reproduce the measured values quite well. By comparing with the individual $LS\pi$ contributions to the total channel cross section in this region, it is quite evident that this is a $^2D^e$ resonance.

A similar comparison at somewhat higher energy is given in Fig. 13, where the calculations reproduce quite well the energy and shape of the strong observed resonance. The existence of a second weak peak predicted by the calculations at about 0.3 eV lower energy is not fully confirmed by the

TABLE IV. Binding energies (in eV) of the $2l2l'$ ionization thresholds relative to the first excited state $1s^2 2p$ in atomic lithium.

State	$2s^2\,{}^1S$	$2s2p\,{}^3P$	$2p^2\,{}^3P$	$2p^2\,{}^1D$	$2s2p\,{}^1P$	$2p^2\,{}^1S$
E (eV)	149.507	150.347	152.607	153.380	153.681	157.340

experimental data where a weak structure can be seen 0.15 eV lower photon energy. From the individual $LS\pi$ cross sections shown, it is clear that the larger resonance is $^2P^e$.

These same resonances also appear in the $1s2p\,{}^1P^o$ cross section, and a comparison of the R-matrix result with experiment [14,19] is shown in Fig. 14, where the theoretical contributions from the various $LS\pi$ subchannels are seen. Agreement between theory and experiment is about the same as for the $^3P^o$ case.

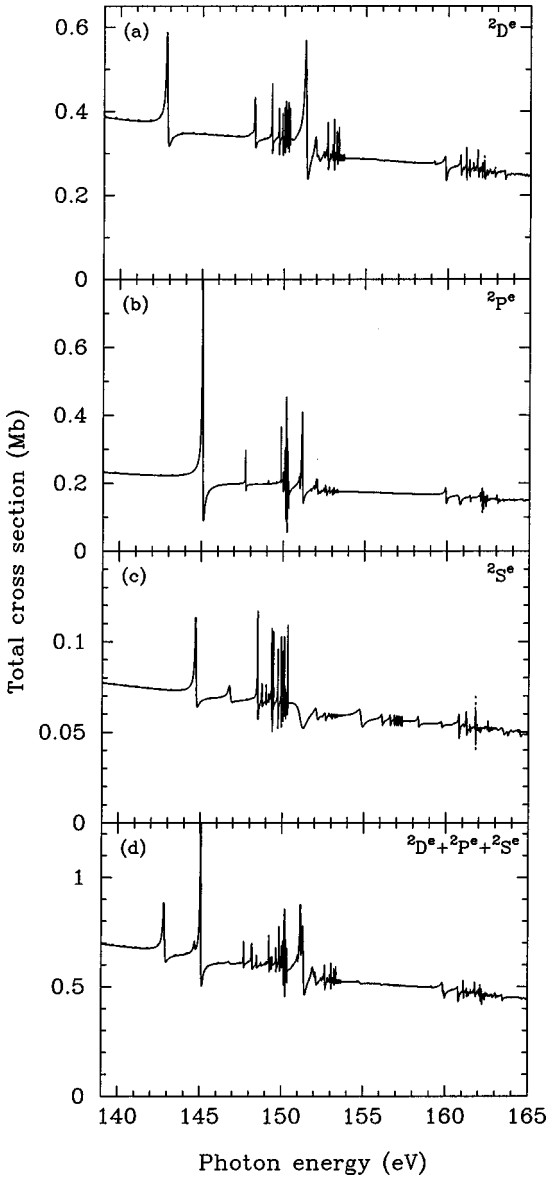

FIG. 11. Contribution of each $SL\pi$ final state to the total photoionization cross section from the $1s^2 2p$ Li excited state in the 140–165 eV photon energy range: (a) $^2D^e$, (b) $^2P^e$, and (c) $^2S^e$. The curve (d) represents the total photoionization cross section. Results in length and velocity forms are superimposed.

Decomposition of the total photoionization cross section into its component $SL\pi$ final states facilitates the determination of resonance positions for each series converging to a $2l2l'$ ionization threshold of atomic lithium. For each $SL\pi$ final state we can determine the quantum defect [20]. For each Rydberg series $(2l2l'^{2S+1}L)nl''^2L^e$, an effective quantum number n^* is defined as

$$(n^*)^{-2}=E_{\text{thres}}(2l2l'^{2S+1}L')-E[(2l2l'^{2S+1}L')nl''^2L^e], \tag{5}$$

where energies are in Rydberg units, $n^*\equiv n-\mu_n$, and μ_n is the quantum defect. The energies $E[(2l2l'^{2S+1}L')nl''^2L^e]$ are determined using the calculated partial cross sections in the various subchannels, which allows the positions of the resonances to be clearly determined without ambiguity. We also used the eigenphase derivative technique [21] as a

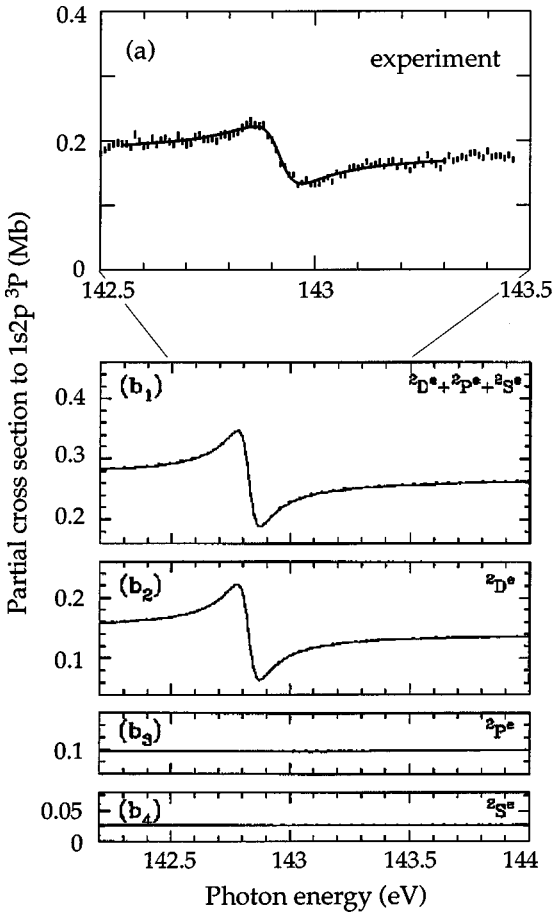

FIG. 12. Comparison between experimental measurements from Ref. [19] (a) and present theoretical partial cross section (b_1) to the $1s2p\,{}^3P$ final ionic state from the $1s^2 2p$ Li excited state in the vicinity of the $2s2p^2\,{}^2D^e$ resonance. Curves (b_2), (b_3), and (b_4) represent the different contributions from each $SL\pi$ final state to the total cross section, respectively.

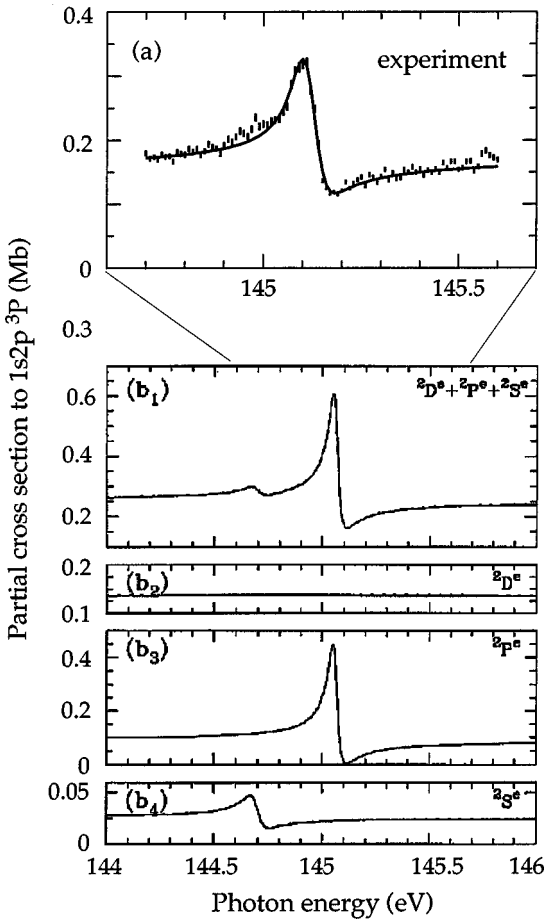

FIG. 13. Comparison between experimental measurements from Refs. [14] and [19] (a) and present theoretical total cross section (b_1) to the $1s2p\ ^3P$ final ionic state from the $1s^22p$ Li excited state in the vicinity of the $2s2p^2\ ^2P^e$ resonance. Curves (b_2), (b_3), and (b_4) represent the different contributions from each $SL\pi$ final state to the total cross section, respectively.

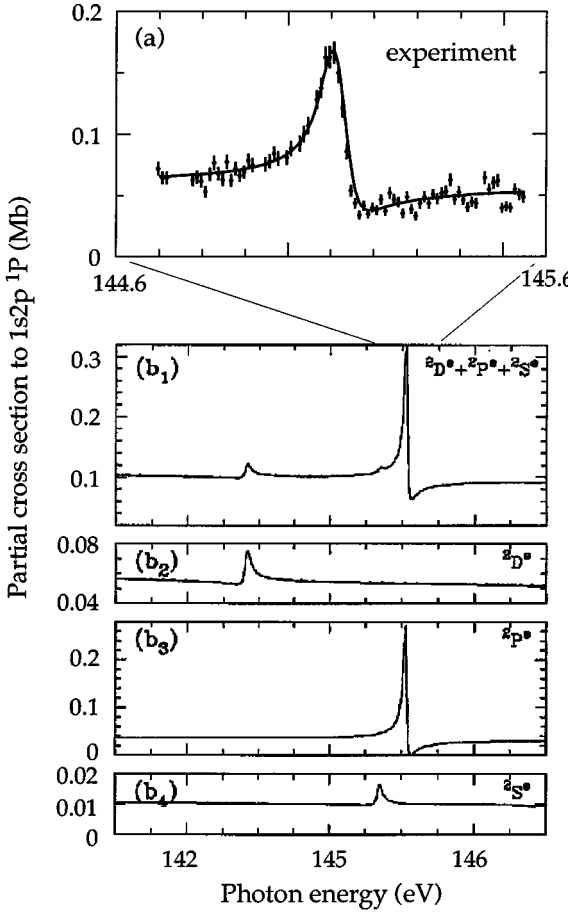

FIG. 14. Comparison between experimental measurements from Refs. [14] and [19] (a) and present theoretical total cross section (b_1) to the $1s2p\ ^1P$ final ionic state from the $1s^22p$ Li excited state in the vicinity of the $2s2p^2\ ^2L^e$ resonances. Curves (b_2), (b_3), and (b_4) represent the different contributions from each $SL\pi$ final state to the total cross section, respectively.

check, and for weak resonances whose positions are not obvious from our cross sections. It is worthwhile to point out that, using these more sophisticated methods, we have revised the assignments of higher-energy resonances from previous work [14]. Table V gives the position of the resonances along with the effective quantum number, n^*, for the 19 *ns*, *np*, *nd*, and *nf* series of $2l2l'n''l''$ of resonances leading up to the $2s^2(^1S)$, $2p^2(^1S,^3P,^1D)$, and the $2s2p(^{1,3}P)$ autoionizing states of the Li^+ ion. Table V shows that there are significant series perturbations among the resonances, with the strong resonances perturbing the weak ones. For example, the weak $2s^2(^1S)7d\ ^2D$ resonance is perturbed by the very much stronger $2s2p(^3P)4p\ ^2D$ so that the quantum defect, n-n^*, for the weaker resonance does not follow the rest of the series. In addition, the $2s^2(^1S)7d\ ^2D$ resonance is much stronger than the other members of the series. This is because, in the interaction with the stronger series, the weak resonance has ''borrowed'' a bit of the oscillator strength of the strong one, thereby proportionally increasing the strength of the weak resonance markedly without materially affecting the strong one. Many other examples of this phenomenon are revealed in Table V.

The quantum defects n-n^* can be obtained from Table V for each of the series; owing to the perturbations, the quantum defects along each series do not approach an asymptotic limit as quickly as for an isolated series, but a certain general regularity is seen. All of the *ns* series have substantial quantum defects owing to the penetration of *ns* orbitals into the core. The largest quantum defects are for the $2s^2(^1S)ns\ ^2S$ series owing to the large attractive $2s$-ns exchange term. For the three $2p^2ns$ series, the ^2P and ^2D quantum defects still vary in the range shown in Table V owing to nearby series perturbations. The ^2S quantum defects have stabilized at 0.68, showing that this series is somewhat less bound than the $2s^2ns$ series; this is because the $2s$-ns exchange term in the latter is more attractive than $2p$-ns exchange arising in the $2p^2ns$ series. For the six strong $2s2pnp$ resonance series, it is largely the $2p$-np exchange and direct quadrupole terms which determine the relative quantum defects. Since *np* functions are not so penetrating, these terms are significantly more important than in the *ns* case, and the quantum defects vary far more widely among the various *np* series.

The seven *nd* series all have very small quantum defects, being very nonpenetrating, which are determined by the $2p$-nd direct and exchange interactions. Note that some of the quantum defects are negative, indicating that the interac-

TABLE V. Excitation energies from initial state $1s^2 2p$, effective quantum numbers (n^*), and assignment of the lower $2l2l'n''l''$ hollow atom resonances, along with the labels given in Figs. 15 and 16. Also shown are the theoretical results inferred from Ref. [22].

				$^2D^e$				
		$2s^2(^1S)nd$		n^*		$2s2p(^3P)np$		n^*
n		E (eV)	n^*	[22]		E (eV)	n^*	[22]
2					p_2	142.816	1.344	
3	d_3	147.978	2.984	2.968	p_3	148.197	2.516	2.509
4	d_4	148.636	3.953	3.944	p_4	149.249	3.522	3.507
5	d_5	148.950	4.944	4.924	p_5	149.676	4.503	4.500
6	d_6	149.120	5.933	5.911	p_6	149.895	5.489	5.486
7	d_7	149.221	6.890	6.888	p_7	150.022	6.474	6.471
8	d_8	149.293	7.964	7.976	p_8	150.102	7.462	7.459
∞		149.507 17				150.346 65		
		$2s2p(^1P)np$		n^*		$2p^2(^1D)ns$		n^*
n		E (eV)	n^*	[22]		E (eV)	n^*	[22]
3	p'_3	151.329	2.405	2.381	s_3	150.516	2.180	2.194
4	p'_4	152.472	3.356	3.415	s_4	152.081	3.237	3.210
5	p'_5	152.968	4.367	4.472	s_5	152.669	4.375	4.418
6	p'_6	153.230	5.490	5.424	s_6	152.893	5.291	5.275
7	p'_7	153.353	6.437	6.447	s_7	153.047	6.401	6.169
8	p'_8	153.437	7.460	7.447	s_8	153.123	7.282	7.347
∞		153.681 29				153.379 92		
		$2p^2(^1D)nd$		n^*		$2p^2(^1S)nd$		n^*
n		E (eV)	n^*	[22]		E (eV)	n^*	[22]
3	d'_3	151.924	3.057	3.097	d''_3	155.829	3.000	3.071
4	d'_4	152.527	3.994	3.836	d''_4	156.468	3.950	3.974
5	d'_5	152.833	4.987	5.010	d''_5	156.777	4.916	4.921
6	d'_6	153.014	6.102	5.886	d''_6	156.949	5.910	5.898
7	d'_7	153.104	7.017	7.047	d''_7	157.053	6.889	6.888
8	d'_8	153.164	7.945	7.997	d''_8	157.121	7.884	7.883
∞		153.379 92				157.340 07		
		$2p^2(^3P)nd$		n^*		$2s2p(^3P)nf$		n^*
n		E (eV)	n^*	[22]		E (eV)	n^*	[22]
3	d^*_3	151.184	3.093	3.130				
4	d^*_4	151.784	4.068	4.103	f_4	149.496	4.000	4.003
5	d^*_5	152.076	5.064	5.094	f_5	149.804	5.006	4.998
6	d^*_6	152.238	6.080	6.086	f_6	149.969	6.002	5.995
7	d^*_7	152.335	7.079	7.082	f_7	150.069	6.999	6.993
8	d^*_8	152.398	8.078	8.082	f_8	150.134	7.998	7.992
∞		152.606 57				150.346 65		
		$2s2p(^1P)nf$		n^*				
n		E (eV)	n^*	[22]				
4	f'_4	152.847	4.038	3.984				
5	f'_5	153.141	5.018	4.950				
6	f'_6	153.301	5.986	5.917				
7	f'_7	153.404	7.002	6.925				
8	f'_8	153.469	7.999	7.925				
∞		153.681 29						

TABLE V. (*Continued*).

				$^2P^e$				
		$2s2p(^3P)np$		n^*		$2p^2(^3P)ns$		n^*
n		E (eV)	n^*	[22]		E (eV)	n^*	[22]
2	p_2	145.062	1.064					
3	p_3	147.700	2.266	2.265	s_3	150.207	2.380	2.390
4	p_4	149.095	3.296	3.288	s_4	151.517	3.534	3.526
5	p_5	149.606	4.285	4.287	s_5	151.915	4.436	4.441
6	p_6	149.857	5.269	5.271	s_6	152.144	5.423	5.430
7	p_7	149.997	6.241	6.241	s_7	152.273	6.384	6.385
8	p_8	150.084	7.195	7.190	s_8	152.353	7.328	7.314
∞		150.346 65				152.606 57		
		$2p^2(^3P)nd$		n^*		$2p^2(^1D)nd$		n^*
n		E (eV)	n^*	[22]		E (eV)	n^*	[22]
3	d_3	151.012	2.921	2.931	d'_3	151.986	3.124	3.260
4	d_4	151.725	3.930	3.925	d'_4	152.658	4.343	4.338
5	d_5	152.042	4.911	4.885	d'_5	152.855	5.092	5.127
6	d_6	152.218	5.921	5.911	d'_6	152.988	5.892	5.918
7	d_7	152.321	6.909	5.896	d'_7	153.113	7.141	7.229
8	d_8	152.387	7.889	7.862	d'_8	153.167	8.012	8.120
∞		152.606 57				153.379 92		
		$2s2p(^1P)np$		n^*				
n		E (eV)	n^*	[22]				
3	p'_3	151.167	2.507	2.311				
4	p'_4	152.439	3.309	3.232				
5	p'_5	153.038	4.599	4.460				
6	p'_6	153.228	5.479	5.497				
7	p'_7	153.356	6.467	6.492				
8	p'_8	153.438	7.476	7.500				
∞		153.681 29						
				$^2S^e$				
		$2s^2(^1S)ns$		n^*		$2s2p(^3P)np$		n^*
n		E (eV)	n^*	[22]		E (eV)	n^*	[22]
2					p_2	144.686	1.550	
3	s_3	146.784	2.235	2.243	p_3	148.489	2.707	2.694
4	s_4	148.216	3.247	3.181	p_4	149.358	3.709	3.680
5	s_5	148.752	4.244	4.228	p_5	149.729	4.694	4.684
6	s_6	149.007	5.214	5.212	p_6	149.926	5.690	5.681
7	s_7	149.153	6.202	6.205	p_7	150.042	6.686	6.677
8	s_8	149.244	7.191	7.198	p_8	150.116	7.683	7.676
∞		149.507 17				150.346 65		
		$2p^2(^1D)nd$		n^*		$2s2p(^1P)np$		n^*
n		E (eV)	n^*	[22]		E (eV)	n^*	[22]
3	d_3	152.102	3.263	3.264	p'_3	151.168	2.327	2.355
4	d_4	152.635	4.273	4.273	p'_4	152.437	3.307	3.249
5	d_5	152.863	5.131	5.147	p'_5	152.958	4.338	4.415
6	d_6	153.031	6.244	5.957	p'_6	153.206	5.351	5.354
7	d_7	153.114	7.162	7.186	p'_7	153.342	6.334	6.325
8	d_8	153.170	8.056	8.134	p'_8	153.425	7.290	7.325
∞		153.379 92				153.681 29		

TABLE V. (*Continued*).

n		$2p^2(^1S)ns$ E (eV)	n^*	n^* [22]
3	s_3'	154.827	2.327	2.355
4	s_4'	156.113	3.329	3.335
5	s_5'	156.614	4.329	4.341
6	s_6'	156.860	5.326	5.341
7	s_7'	156.700	6.325	6.341
8	s_8'	157.086	7.324	7.341
∞		157.340 07		

tions are sometimes repulsive making the *nd* electron less bound than in the hydrogen atom. Finally, the two *nf* series, being completely nonpenetrating, have very small interaction with the core, so that the quantum defects are essentially zero and the *nf* orbitals are hydrogenic.

Also shown in Table V are the n^* values for these resonances obtained by a different *R*-matrix calculation [22]. As seen in Table V, agreement is excellent for almost all of the resonances. For the few where there is a disagreement, we have no explanation for the differences.

Using the saddle-point method, Chung and Gou [23] calculated nonrelativistic and relativistic energies of some low-lying triply excited even-parity resonances. Relativistic effects are negligible compared to the precision of the present calculations. Chung and Gou's results (not shown) are in very good agreement with ours. A full study of the resonances and the details of the series perturbations and asymptotic quantum defects is beyond the scope of this paper and will be presented elsewhere.

Figures 15 and 16 show the total and $LS\pi$ partial cross-section results along with the assignment of each resonance from Table V over the incident photon energy ranges of 147.5–150.5 eV (Fig. 15) and 150.5–153.5 eV (Fig. 16).

III. CONCLUSION

The present *R*-matrix calculation deals with photoionization from the excited states $1s^22p\,^2P^o$ and $1s^23p\,^2P^o$ of neutral lithium for incident photon energies up to 165 eV. This energy range allows us to account for resonances due to even-parity excited states corresponding to $nln'l'n''l''\ ^2L^e$ for $n=1$ and 2. In the *R*-matrix code, the CC and CI expansions are those used in the previous study of hollow lithium states from the ground state [2].

Partial and total photoionization cross sections are shown in some detail. For each of them, the final cross section can be divided into three components which correspond to each final state $SL\pi$: $^2D^e$, $^2P^e$, or $^2S^e$. To our knowledge, these

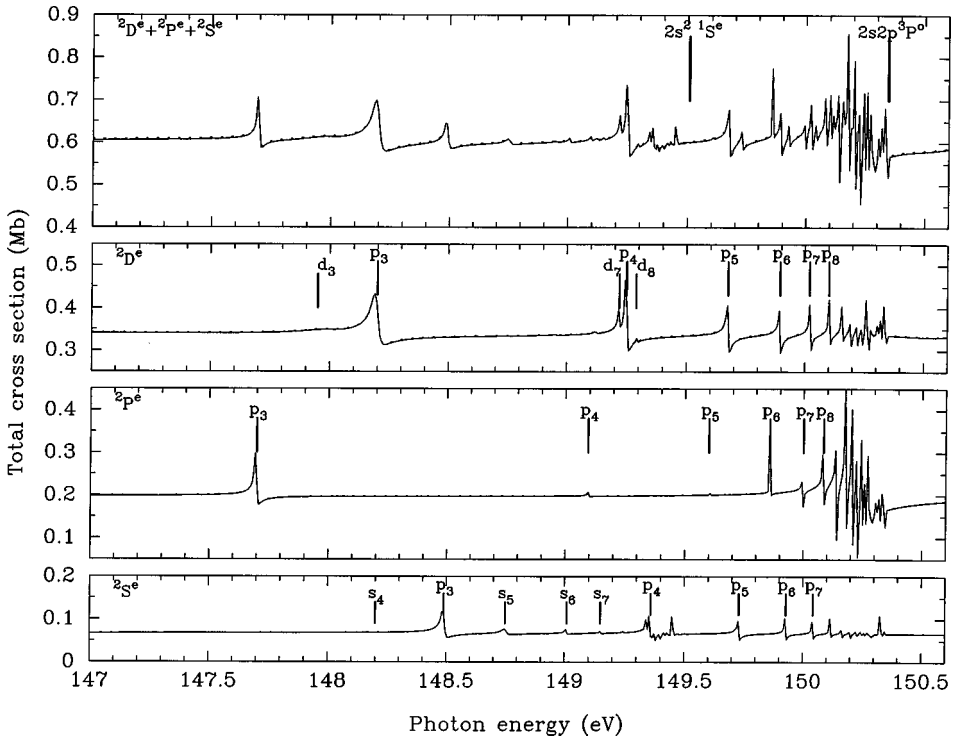

FIG. 15. Present assignment, shown in Table V, of the theoretical Rydberg series running up to the $2s^2\ ^1S^e$ threshold (149.507 eV) and to the $2s2p\ ^3P^o$ threshold (150.347 eV) in the 147–150.5 eV incident photon energy range, from present *ab initio* calculations. Assignments are only given for the separated $SL\pi$ contributions and the different labels correspond to the respective $SL\pi$ in Table V.

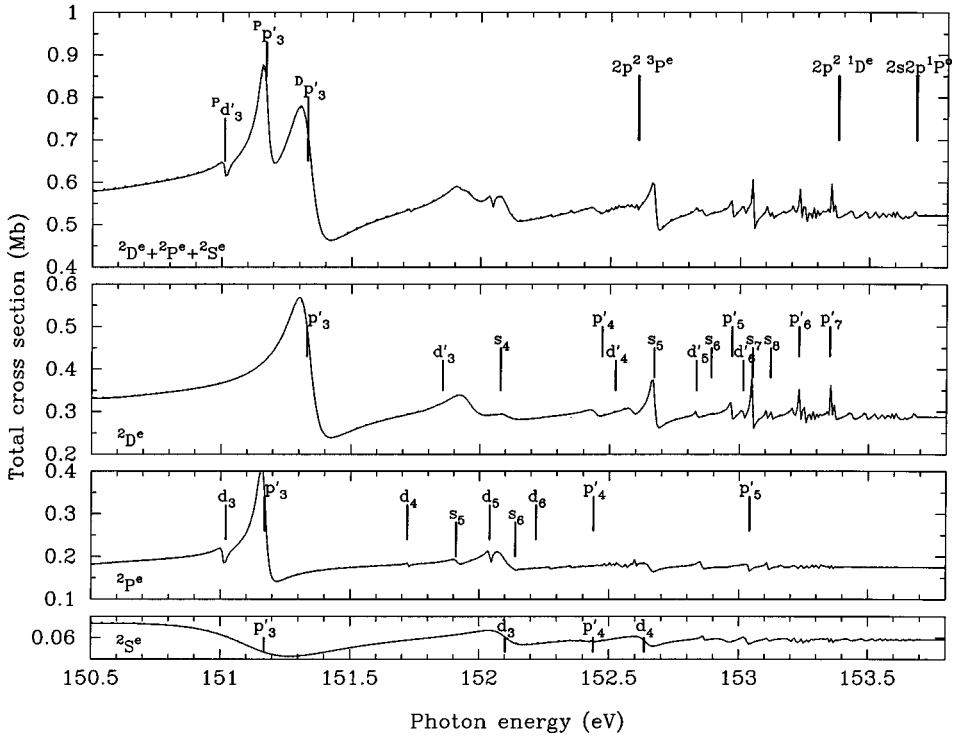

FIG. 16. Present assignment, shown in Table V, of the theoretical Rydberg series running up to the $2p^2\,^3P^e$ threshold (152.606 eV), to the $2p^2\,^1D^e$ threshold (153.380 eV), and to the $2s2p\,^1P^o$ threshold (153.681 eV) in the 150.5–153.8 eV incident photon energy range, from present *ab initio* calculations. Assignments are only given for the separated $SL\pi$ contributions and the different labels correspond to the respective $SL\pi$ in Table V.

are the first theoretical results obtained for photon energies including the $2ln'l'n''l''$ resonances. In the photon energy range outside the resonances, partial cross sections are compared with previous MCHF calculations [9]; agreement is good far above threshold but, at low energies, their results are quite different from the present ones. In the region of even-parity hollow atomic states, the present calculated partial cross sections compare well with measurements.

Branching ratios among partial cross sections and asymmetry parameters are also given for certain cases. These results confirm the increasing importance of the shake-up processes when the initial state is more highly excited. As an example, the cross-section ratio between the first shake-up satellite line and the direct main line is equal to 0.6 for $1s^22p$ and 5.0 for $1s^23p$.

Finally, an assignment is given for low-lying resonances calculated in the 140–160 eV photon energy range which are converging to a $2l2l'^{2S+1}L^{o,e}$ ionization threshold of atomic lithium. This assignment is possible owing to the facility of the *R*-matrix code to separate each partial cross section for each $SL\pi$ final state. The energy values thus obtained for the $2l2l'n''l''\ ^2L^e$ autoionizing states are in excellent agreement with those obtained from the saddle-point technique [23].

ACKNOWLEDGMENTS

The calculations were carried out partly on the CRAY YMP/2E computer at the IMT, Marseille (France), which was supported by the Conseil Régional Provence-Alpes-Côte d'Azur, and partly on the CRAY C98 (IDRIS-France Project No. 940052). We thank A.F. Starace for important discussions concerning the phases of certain matrix elements. A.H. acknowledges partial funding from the EC HCM Network under Contract No. CHRX-CT93-0361. H.L.Z. and S.T.M. acknowledge partial funding from the NSF and NASA. H.L.Z. acknowledges partial funding from the Center for the Theoretical Study of Physical Systems (CTSPS) at Clark Atlanta University. F.J.W. acknowledges partial funding from the Centre d'Etudes de Limeil-Valenton (DRIF) under Contract Nos. 6R1609MF and 8M3095/PB.

[1] L. Vo Ky, P. Faucher, A. Hibbert, J.-M. Li, Y.-Z. Qu, J. Yan, J. C. Chang, and F. Bely-Dubau, Phys. Rev. A **57**, 1045 (1998).

[2] L. Vo Ky, P. Faucher, H. L. Zhou, A. Hibbert, Y.-Z. Qu, J. M. Li, and F. Bely-Dubau, Phys. Rev. A **58**, 3688 (1998).

[3] L. M. Kiernan, E. T. Kennedy, J.-P. Mosnier, J. T. Costello, and B. F. Sonntag, Phys. Rev. Lett. **72**, 2359 (1994).

[4] Y. Azuma, S. Hasegawa, F. Koike, G. Kutluk, T. Nagata, E. Shigemasa, A. Yagishita, and I. A. Sellin, Phys. Rev. Lett. **74**, 3768 (1995).

[5] L. M. Kiernan, M.-K. Lee, B. F. Sonntag, P. Sladeczek, P. Zimmermann, E. T. Kennedy, J.-P. Mosnier, and J. P. Costello, J. Phys. B **28**, L161 (1995).

[6] L. Journel, D. Cubaynes, J.-M. Bizau, S. Al Moussalami, B. Rouvellou, F. J. Wuillemier, L. Vo Ky, P. Faucher, and A. Hibbert, Phys. Rev. Lett. **76**, 30 (1996).

[7] S. Diehl, D. Cubaynes, J.-M. Bizau, L. Journel, B. Rouvellou, S. Al Moussalami, F. J. Wuillemier, E. T. Kennedy, N. Berrah, C. Blancard, T. J. Morgan, J. Bozek, A. S. Schlachter, L. Vo Ky, P. Faucher, and A. Hibbert, Phys. Rev. Lett. **76**, 3915 (1996).
[8] K. T. Chung, Phys. Rev. Lett. **78**, 1416 (1997); Phys. Rev. A **57**, 3518 (1998).
[9] Z. Felfli and S. T. Manson, Phys. Rev. Lett. **68**, 1687 (1992).
[10] L. Journel, Ph.D. thesis, University Paris–Sud, 1995 (unpublished).
[11] D. Cubaynes, J.-M. Bizau, F. J. Wuilleumier, B. Carré, and F. Gounand, Phys. Rev. Lett. **63**, 2460 (1989).
[12] M. Richter, J.-M. Bizau, D. Cubaynes, T. Menzel, and F. J. Wuilleumier, Europhys. Lett. **12**, 35 (1990).
[13] F. J. Wuilleumier, D. Cubaynes, and J.-M. Bizau, in *Atomic and Molecular Physics*, edited by C. Cisneros, T. J. Morgan, and I. Alvarez (World Scientific, Singapore, 1991), pp. 474–495.
[14] D. Cubaynes, S. Diehl, L. Journel, B. Rouvellou, J.-M. Bizau, S. Al Moussalami, F. J. Wuillemier, N. Berrah, L. Vo Ky, P. Faucher, A. Hibbert, C. Blancard, E. T. Kennedy, T. J. Morgan, J. Bozek, and A. S. Schlachter, Phys. Rev. Lett. **77**, 2194 (1996).
[15] A. Hibbert, Comput. Phys. Commun. **9**, 141 (1975).
[16] S. T. Manson and A. F. Starace, Rev. Mod. Phys. **54**, 389 (1982).
[17] J. Cooper and R. N. Zare, in *Lectures in Theoretical Physics*, edited by S. Geltman, K. T. Mahanthappa, and W. E. Britten (Gordon and Breach, New York, 1969), Vol. XI-C, pp. 317–337.
[18] S. T. Manson, J. Electron Spectrosc. Relat. Phenom. **1**, 413 (1972).
[19] S. Diehl, Ph.D thesis, University Paris–Sud, 1998 (unpublished).
[20] M. J. Seaton, Proc. Phys. Soc. London **88**, 801 (1966).
[21] L. Quigley and K. Berrington, J. Phys. B **29**, 4529 (1996).
[22] K. Berrington and S. Nakazaki, J. Phys. B **31**, 313 (1998).
[23] K. T. Chung and B. C. Gou, Phys. Rev. A **52**, 3669 (1995).
[24] I. Johansson, Ark. Fys. **15**, 169 (1959).